J Artif Organs (2014) 17:178–185
DOI 10.1007/s10047-014-0755-3

ORIGINAL ARTICLE

Others

The effect of turbulent viscous shear stress on red blood cell hemolysis

Jen-Hong Yen · Sheng-Fu Chen · Ming-Kai Chern · Po-Chien Lu

Received: 4 February 2013 / Accepted: 14 January 2014 / Published online: 12 March 2014

Abstract Non-physiologic turbulent flow occurs in medical cardiovascular devices resulting in hemodynamic stresses that may damage red blood cells (RBC) and cause hemolysis. Hemolysis was previously thought to result from Reynolds shear stress (RSS) in turbulent flows. A more recent hypothesis suggests that turbulent viscous shear stresses (TVSS) at spatial scales similar in size to RBCs are related to their damage. We applied two-dimensional digital particle image velocimetry to measure the flow field of a free-submerged axisymmetric jet that was utilized to hemolyze porcine RBCs in selected locations. Assuming a dynamic equilibrium for the sub-grid scale (SGS) energy flux between the resolved and the sub-grid scales, the SGS energy flux was calculated from the strain rate tensor computed from the resolved velocity fields. The SGS stress was determined by the Smagorinsky model, from which the turbulence dissipation rate and then TVSS were estimated. Our results showed the hemolytic threshold of the Reynolds stresses was up to 517 Pa, and the TVSSs were at least an order of magnitude less than the RSS. The results provide further insight into the relationship between turbulence and RBC damage.

Keywords Hemolysis · Sub-grid scale · Turbulent dissipation rate · Viscous dissipative stresses · Particle image velocimetry

J.-H. Yen (✉) · P.-C. Lu (✉)
Department of Water Resources and Environmental Engineering, Tamkang University, 151 Ying-Chuan Road, Tamsui, New Taipei 251, Taiwan
e-mail: 899480023@s99.tku.edu.tw

P.-C. Lu
e-mail: lupc@mail.tku.edu.tw

S.-F. Chen
Division of Medical Engineering, National Health Research Institute, Miaoli 350, Taiwan

M.-K. Chern
Department of Chemistry, Tamkang University, New Taipei 251, Taiwan

Introduction

As blood flows through artificial devices, such as left ventricular assist devices, artificial valves, and bypass tubing, non-physiologic turbulent flow occurs. Consequently, hemodynamic stresses on blood components, specifically red blood cells (RBCs) and platelets, may lead to hemolysis and thrombosis. Early researchers focused on studying the underlying mechanism of hemolysis and revealed that RBCs are damaged through regions of high shear stresses in the flow fields [1]. Subsequent research focused on two factors: the magnitude of shear stress and the exposure time in the flow fields. The threshold levels of RBC damage and the corresponding estimated exposure times from selected literature are shown in Table 1.

In laminar flow, the viscous stress tensor is computed by:

$$\tau_{ij,\mathrm{lam}} = \mu\left(\frac{\partial u_i}{\partial x_j} + \frac{\partial u_j}{\partial x_i}\right) \quad (1)$$

where μ is the dynamic viscosity, u_i and u_j are the real instantaneous velocities, and i and j take on the coordinate designations of x, y, and z. When $i \neq j$, $\tau_{ij,\mathrm{lam}}$ may be interpreted as shear stress.

In turbulent flow, the turbulence stresses are designated by:

Table 1 Threshold level of RBC damage and corresponding estimated exposure time from selected literature

Type of exposure	Order of magnitude of exposure time (s)	Threshold level of damage (Pa)	References and comments
Laminar flow			
Concentric cylinder	120	300	Nevaril et al. [2]
Concentric cylinder	120	150	Leverett et al. [3]
Concentric cylinder	100–200	100	Sutera et al. [4]
Concentric cylinder	120	150	Hellums and Brown [1]
Oscillating wire	10^{-4}	560	Williams et al. [5]
Oscillating bubble	10^{-3}	450	Rooney [6]
Turbulent flow			
Turbulent jet	10^{-6}	4000	Forstrom [7]
Concentric cylinder	240	250	Sutera and Mehrjardi [8]
Turbulent jet	10^{-5}	400	Sallam and Hwang [9]
Turbulent jet	–	600	Grigioni et al. [10] Stress analysis of Sallam and Hwang's [9] measurement
Turbulent jet	–	800	Lu et al. [11] re-examine flow features of Sallam and Hwang's [9] measurement

$$\tau_{ij,\text{turb}} = -\rho\overline{u_i' u_j'} \tag{2}$$

and are often called Reynolds stresses, where ρ is the fluid density, and u_i' and u_j' are both fluctuating velocities. The Reynolds stresses have both normal and tangential components and are symmetric: $\tau_{ij,\text{turb}} = \tau_{ji,\text{turb}}$. The normal components are obtained by setting $i = j$. In jet flow, these normal stresses contribute little to the transport of momentum. In contrast, the tangential components (when $i \neq j$) are shear stresses that play a dominant role in the theory of momentum transport by turbulent motion. The shear stress component $-\rho\overline{u_1' u_2'}$ (i.e., $-\rho\overline{u'v'}$) is more important since it is one order of magnitude higher than the other component [12, 13]. For simplicity, this component will be named the Reynolds shear stress (RSS).

In turbulent flow, RBCs would only be damaged when the scale of the smallest vortices (Kolmogorov scale) approaches the scale of RBCs. However, the RSS calculated in the flow field belongs to macro scale and therefore should not be considered the real stress causing hemolysis [14, 15]. Actually, the RSS is derived from taking the Reynolds average to the Navier–Stokes equation, so it is a statistical term and not a physical shear stress. Grigioni et al. [10] pointed out that hemolysis would increase with the RSS in the experiment by Sallam and Hwang [9], thus indicating there was some contribution by RSS. Jones [14] concluded that the hemolytic force should be turbulent viscous shear stress (TVSS), which is proportional to the square root of the turbulent energy viscous dissipation. Quinlan and Dooley [16] applied the LDV experiment data by Liu et al. [17] and elongated the turbulent energy spectrum to higher frequency at Kolmogorov scale, and they additionally considered the square of the function of flow-induced viscous shear stress (VSS) on a sphere in simple laminar shear flow or the shear on a sphere oscillating in still fluid as a weight. Antiga and Steinman [18] calculated VSS by expanding upon the spectrum elongation method by Quinlan and Dooley [16] and taking into account the relative velocities between two neighboring eddies and the distance between two red cells within high RBC concentration.

Based on the above research, TVSS is produced by interactions between the velocity gradients of small scale vortices and the viscosity of fluid, and this stress could be regarded as a real physical force in hemolysis. TVSS can be calculated by turbulent dissipation rates, which occur at the Kolmogorov length scale and therefore are very difficult to directly measure. Sheng et al. [19] measured the flow field of a stirred vessel by PIV and estimated turbulent dissipation rates. They assumed the flow field was in dynamic equilibrium, and dissipation rates could be estimated at a smaller scale by applying a large eddy simulation (LES) and sub-grid scale (SGS) model, due to the limited spatial resolution of PIV.

In this study, we apply PIV to measure the entire flow field of a jet and the large eddy PIV method of Sheng et al. [19]. This method allows the real velocity to be considered as two terms: the PIV resolved velocity of large scale and the unresolved velocity of small scale. Based on dimensional analysis, when the local integral length scale is much larger than the distance between two measurement points, the real velocity approximates the PIV resolved velocity of large scale [20]. Therefore, from the kinetic energy transport equation [19], the Reynolds averaged SGS dissipation rate can be directly calculated from the PIV resolved velocity field and then yield the turbulent dissipation rate. We can then directly compute the TVSS from the turbulent dissipation rates, the fluid density (ρ), and the dynamic viscosity of fluid (μ), and then estimate whether RBCs would be damaged in the flow fields across a free axisymmetric jet.

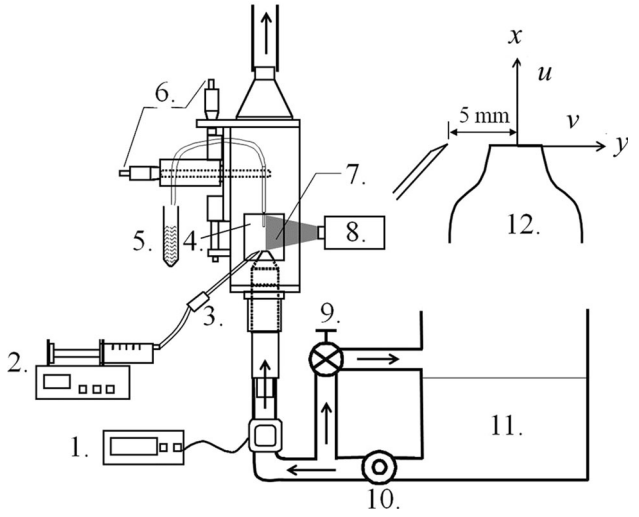

Fig. 1 Schematic drawing of experimental setup. *1* ultrasonic flowmeter, *2* syringe pump, *3* hypodermic needle, *4* aspirator tube, *5* blood sample, *6* aspirator tube motion mechanism, *7* jet image area, *8* digital particle image velocimetry, *9* diverter valve, *10* centrifugal pump, *11* reservoir, *12* geometry (with dimensions) of the jet and blood injection arrangement

Materials and methods

Flow apparatus

RBCs were sampled in the jet flow field at selected locations where the streamwise mean velocity and the RSS were experimentally predetermined. Figure 1 shows the test section that was designed to facilitate the flow configuration of a free-submerged axisymmetric turbulent jet with a 4 mm diameter nozzle (D) mounted on an adjustable nozzle holder. A Plexiglas rectangular section (85 × 85 × 250 mm) with two sides of optic silicon glass allowed for flow field measurements. The blood samples were aspirated through a 1 mm diameter tube mounted on another 2.5 mm ID tube holder. The aspirator was mounted on a holding plate that was vertically and horizontally positioned using threaded shafts through a fixed frame and monitored with dial micrometers. The blood was loaded into a 50 cc standard syringe connected to a syringe pump. The blood was injected with a 16 G hypodermic needle with an outer diameter of 1.27 mm and the needle tip positioned 5 mm from the jet flow center on the same horizontal level (Fig. 1). The blood was injected at a velocity of 0.42 m/s, in comparison to the jet flow velocity of 8–11 m/s, and any effects on the flow field were negligible. As for the aspirator, Sallam and Hwang [9] used the same sized tube and found any effects on flow field calculations to be <5 %. With a larger jet flow diameter of 4 mm, as opposed to 3 mm in their study, we can be certain that any effects from the aspirator were <5 %.

PIV measurements

Prior to RBC injection, the jet flow field was carefully surveyed with a digital particle image velocimeter (Powerview Ultrapiv System, TSI Inc., St. Paul, MN). The system included a Nd:YAG laser, a PIVCAM 10–30 CCD video camera, a frame grabber board, a synchronizer, and PIV software Insight 3.31. Particles with 10 μm diameter were seeded in the test fluid and illuminated by a 91 μm thick laser sheet. A CCD took pictures with a video resolution of 1016 × 1000 pixels and an interrogation window of 32 × 32 pixels. The measurement window was 12 × 12 mm. The images were analyzed via two-frame cross-correlation and 50 % overlap, which was chosen to optimize the requirements for data quality and spatial resolution [21]. The PIV spatial resolution was calculated from the above data as $\Delta = 32/1000 \times 12/2 \cong 0.19$ mm. In order to achieve statistical convergence with the PIV measurements, the system took 1000 frames for ensemble average [22].

Measurement planes were positioned along the midline of the jet. PIV measurements were performed in 2 dimensions. Flow field measurements were performed under different jet exit velocities, $U_e = 6.38$, 7.60, 8.60, 9.40, 9.70, 10.00, 10.64, and 11.75 m/s. The corresponding Reynolds numbers based on jet exit velocity and jet diameter were $Re = 25520$, 30400, 34400, 37600, 38800, 40000, 42560, and 47000, respectively. The flow field was measured axially at $x/D = 1$–7, where $x = 0$ is the edge of the jet nozzle opening.

We applied turbulence equations for analysis of the flow fields, which include the averaging of RSS. Based on the studies by Baldwin et al. [23], we modified these stresses to major principal Reynolds shear stresses ($\mathrm{RSS_{maj}}$). The $\mathrm{RSS_{maj}}$ is defined as:

$$\mathrm{RSS_{maj}} = \rho\sqrt{\left(\frac{\overline{u'u'} - \overline{v'v'}}{2}\right)^2 + (\overline{u'v'})^2} \tag{3}$$

Large eddy PIV method

We used the large eddy PIV approach to estimate the dissipation rate, which in turn was used to calculate the TVSS. According to Jones [14], the TVSS is:

$$\tau_v = \mu(\overline{s_{ij}s_{ij}})^{1/2} \tag{4}$$

where μ is the dynamic viscosity of the fluid and s_{ij} is the fluctuating rate of strain. The TVSS can more directly evaluate the shear stresses on RBCs in turbulent flow due to the fluid viscosity. According to Tennekes and Lumley [12], the turbulent dissipation rate is:

$$\varepsilon = 2\nu\overline{s_{ij}s_{ij}} \tag{5}$$

Thus Eq. (4) can be rewritten as:

$$\tau_v = \left(\frac{1}{2}\rho\mu\varepsilon\right)^{1/2} \tag{6}$$

This equation demonstrates that the turbulent dissipation rate is a major component of TVSS. The definition of the dissipation rate includes the spatial derivative of the velocity fluctuation components, which can be provided by PIV, and the use of multi-point statistics.

Due to the limitations of spatial resolution with PIV, it was very difficult to directly measure the smallest scale of vortices in the flow field. As such, we not only adopted the general turbulence equations for calculating RSS, but we also applied the large eddy PIV method proposed by Sheng et al. [19] to estimate the turbulent dissipation rate.

The turbulent kinetic energy is generated at large scales and cascaded to small scales where it is dissipated in the viscous sub-range. In other words, the turbulent kinetic energy is mainly generated at the integral scale and then the same amount of energy is dissipated near the Kolmogorov scale. In between, there is a large region called the inertial sub-range where energy is transferred from large scale to small scale, and hence there is no change of turbulent kinetic energy. Based on this dynamic equilibrium, the SGS energy flux between the resolved and sub-grid scales equals the turbulent dissipation rate.

By this method, the real velocity can be expressed as:

$$u_i = \tilde{u}_i + u_i' \tag{7}$$

where u_i is the real velocity, $\tilde{u}_i$ is the resolved velocity and u_i' is the unresolved velocity.

According to Liu et al. [24], the SGS stress is obtained by the following method. The filter provides a formal definition of the averaging process and separates the resolvable scales from the sub-grid scales. We used filtering to derive the resolvable-scale equations. For incompressible flow, the filtered continuity and Navier–Stokes equations are expressed as:

$$\frac{\partial \tilde{u}_i}{\partial x_i} = 0 \tag{8}$$

$$\frac{\partial \tilde{u}_i}{\partial t} + \frac{\partial}{\partial x_j}(\tilde{u}_i\tilde{u}_j) = -\frac{\partial \tilde{p}}{\partial x_i} + v\frac{\partial^2 \tilde{u}_i}{\partial x_j \partial x_j} - \frac{\partial \tau_{ij}}{\partial x_j} \tag{9}$$

where v is the kinematic viscosity and $\tau_{ij} = \widetilde{u_i u_j} - \tilde{u}_i\tilde{u}_j$ is the SGS stress tensor and must be modeled.

To examine the effect of the SGS stress model on resolved scales, we multiplied Eq. (9) by $\tilde{u}_i$ and contracted to obtain the kinetic energy transport equation for the resolved energy $\tilde{q}^2 = \frac{1}{2}\tilde{u}_i\tilde{u}_i$,

$$\frac{\partial \tilde{q}^2}{\partial t} + \tilde{u}_j\frac{\partial \tilde{q}^2}{\partial x_j} = \frac{\partial}{\partial x_j}\left(-\tilde{p}\tilde{u}_j + \upsilon\frac{\partial \tilde{q}^2}{\partial x_j} - \tau_{ij}\tilde{u}_i\right) - \upsilon\frac{\partial \tilde{u}_i}{\partial x_j}\frac{\partial \tilde{u}_i}{\partial x_j} + \tau_{ij}\tilde{S}_{ij} \tag{10}$$

According to the Smagorinsky model [25], the SGS stress is:

$$\tau_{ij} = -2C_s^2\Delta^2|\tilde{S}|\tilde{S}_{ij} \tag{11}$$

where C_s is the Smagorinsky coefficient, Δ is the distance between two measurement points, $|\tilde{S}| = (2\tilde{S}_{ij}\tilde{S}_{ij})^{1/2}$, and $\tilde{S}_{ij}$ is the resolved scale strain rate tensor which is obtained by the following equation:

$$\tilde{S}_{ij} = \frac{1}{2}\left(\frac{\partial \tilde{u}_i}{\partial x_j} + \frac{\partial \tilde{u}_j}{\partial x_i}\right) \tag{12}$$

Ideally, we would have measured nine components of the strain rate tensor in Eq. (12). However, we could only measure $\tilde{S}_{11}, \tilde{S}_{22}, \tilde{S}_{33} = -(\tilde{S}_{11} + \tilde{S}_{22})$ and $\tilde{S}_{12}$. According to Liu et al. [24], an approximation must be made for the $\tilde{S}_{13}$ and $\tilde{S}_{23}$ elements. Examination of these four known components of dissipation rate tensor revealed that they all had similar distributions and magnitudes. Therefore, we could assume that $\tilde{S}_{23} = \tilde{S}_{13} = \tilde{S}_{12}$.

The last term in Eq. (10) is the SGS dissipation $\varepsilon_{SGS} = -\tau_{ij}\tilde{S}_{ij}$, which represents the energy transfer between resolved and sub-grid scales. As previously described, this term would equal the turbulent kinetic energy dissipated in the smallest scales. Therefore, the turbulent dissipation rate was approximated by computing the ensemble averaged SGS dissipation rate

$$\varepsilon \approx \langle\varepsilon_{SGS}\rangle = \langle-\tau_{ij}\tilde{S}_{ij}\rangle \tag{13}$$

where ‹› denotes ensemble average. We then directly calculated TVSS using Eq. (6).

We also applied the following equation to calculate the two-dimensional TVSS ($TVSS_{2D}$) as described by Jones [14]:

$$\tau_{v,2D} = (\mathrm{RSS}\mu S_{12})^{1/2} \tag{14}$$

where μ is the dynamic viscosity and S_{12} is the strain rate of mean velocity in a homogeneous, two-dimensional shear flow.

Hemolysis experiment

The use of human blood for damage tests is considered disadvantageous by most researchers due to the risk of infection, restricted availability, and relatively high cost. According to Zhang et al. [26], the properties of porcine blood are more similar to human blood than those of other

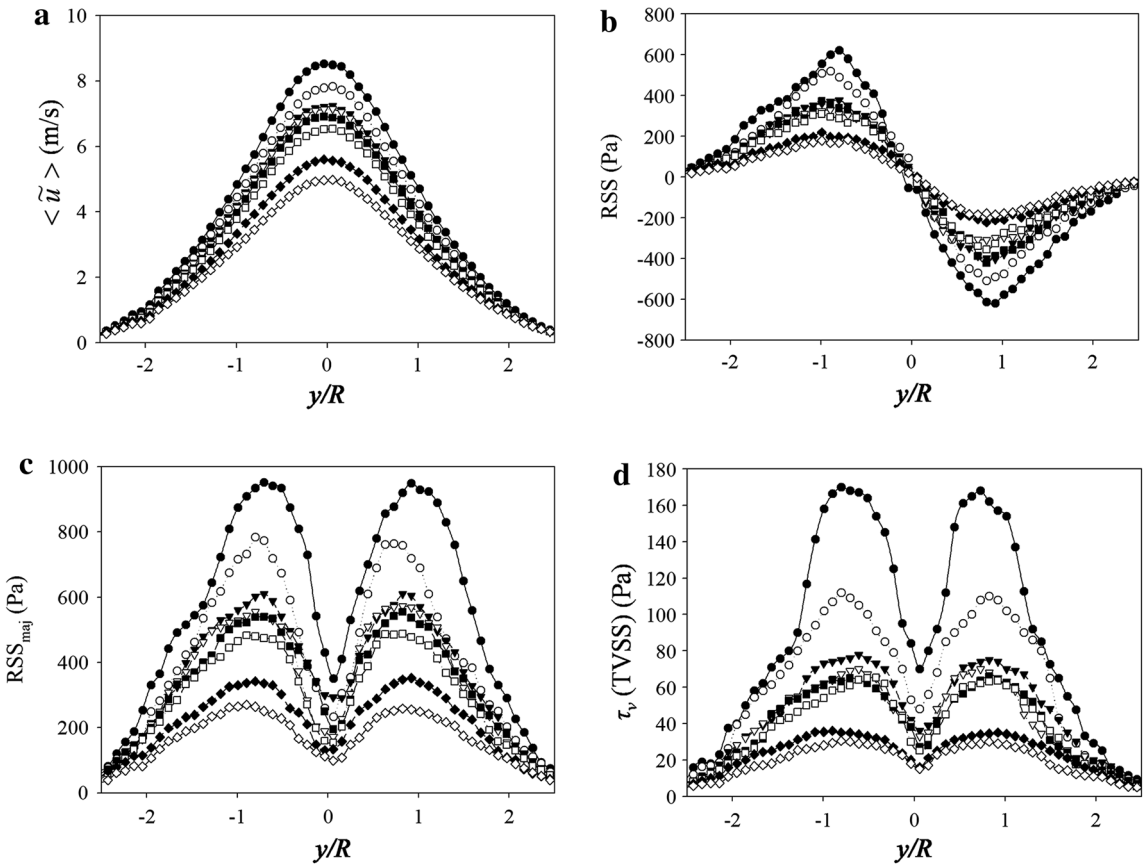

Fig. 2 The flow profiles measured at $x/D = 6$ from the jet nozzle at different Reynolds numbers. **a** Streamwise mean velocity $\langle \tilde{u} \rangle$. **b** Reynolds shear stress (RSS), **c** major Reynolds shear stress (RSS_{maj}), **d** turbulent viscous shear stress τ_v (TVSS). (*Filled circles* $Re = 47000$; *open circles* 42560; *filled triangles* 40000; *open triangles* 38800, *filled squares* 37600; *open squares* 34400, *filled diamonds* 30400; *open diamonds* 25520.)

species. The results from blood tests with porcine blood can then be regarded as a safe estimation for human blood.

Fresh porcine blood samples were collected from a local slaughterhouse. Blood was filtered, anticoagulated with heparin, and filled into sterile blood bottles that were transported within thermo-insulated cases. The blood was washed three times in phosphate-buffered-saline (PBS) solution, and then RBCs were resuspended in PBS to the desired hematocrit. Blood and device temperatures were kept at room temperature throughout the entire test procedure. For each experimental run, a large quantity of PBS was placed in a storage reservoir and then pumped into the test section with a centrifugal pump through the jet exit. Blood was infused into the test section as described earlier, and samples were collected from the flow field with a specially designed aspirator into labeled cuvettes for free-hemoglobin analysis with a spectrophotometer. The rate of rise in free plasma hemoglobin was used as an indicator for hemolysis. Two-point sample technique, presented by Sallam and Hwang [9], was applied to assess the incremental increase in hemolysis between two adjacent locations (subscripts *n* for new and *o* for old) in the following form,

$$Hp\,(\%) = \frac{C_{\mathrm{n}}(1 - Ht_{\mathrm{n}}) - C_{\mathrm{o}}(1 - Ht_{\mathrm{o}})}{C_{\mathrm{ot}} - C_{\mathrm{o}}(1 - Ht_{\mathrm{o}})} \tag{15}$$

where C_{o} and C_{n} are the hemoglobin concentrations at the old position and the new position, respectively; C_{ot} is the hemoglobin concentration of a 100 % hemolyzed sample at the old position; Ht_{o} and Ht_{n} are the hematocrit at the old position and the new position, respectively.

As the RBCs were injected into the flow field, they became entrained in the jet flow and quickly spread through the entire flow field. Most of the RBCs rapidly moved downstream and entered the aspirator. A small portion of the RBCs remained outside the jet flow boundaries and recirculated within areas of slower flow velocity. The exact trajectory of individual RBCs may have been unpredictable, but the two-point sample technique, which assesses different degrees of hemolysis between two immediately adjacent locations

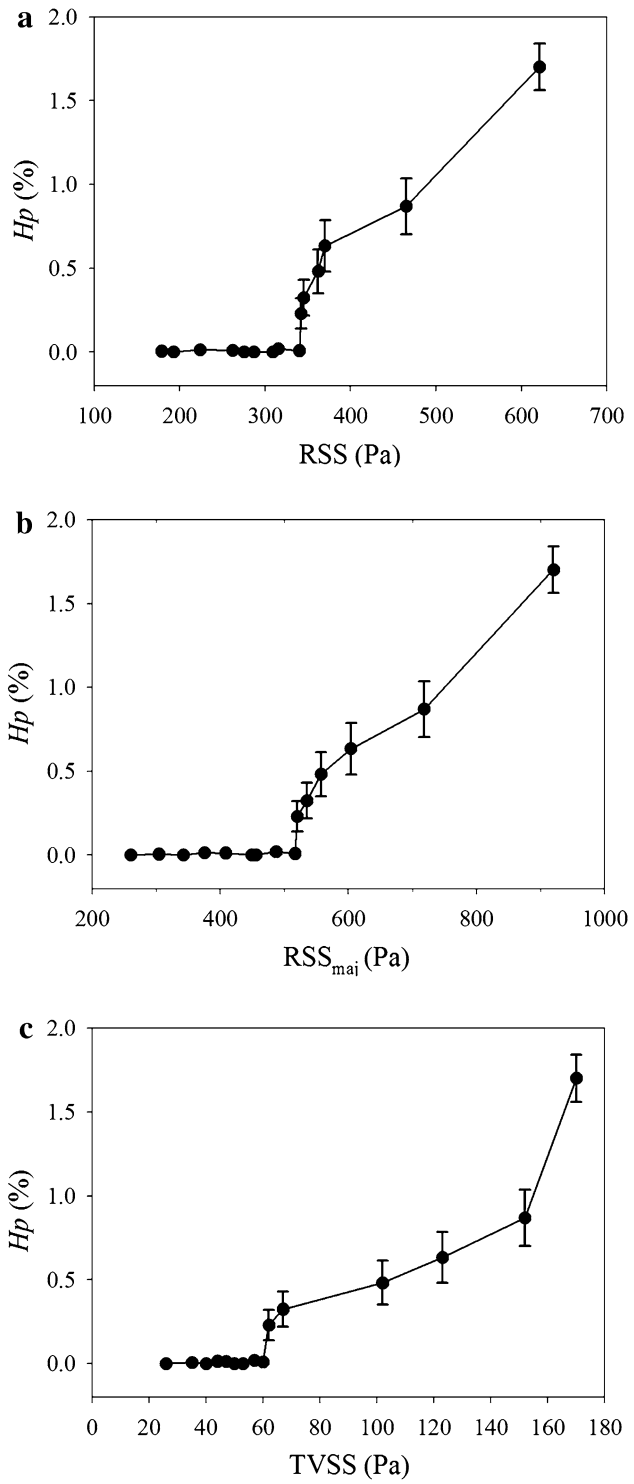

Fig. 3 Red blood cell damage expressed in hemolysis parameter (*Hp %*) as a function of Reynolds shear stress (RSS). **a** Major Reynolds shear stress (RSS_{maj}), **b** and turbulent viscous shear stress τ_v (TVSS), **c** results are presented as mean ± standard error of $n = 8$ experiments

(1 mm apart), eliminated the necessity to track the precise movements between the infusion site and the aspirator.

Results

From the PIV survey of the flow field, the maximum value of RSS was found at $x/D = 6$ and $y/R = 1$. Figure 2a compares the streamwise mean velocity profiles at the downstream distance $x/D = 6$ for our Reynolds numbers ranging from 25520 to 47000. The radial profiles of RSS at $x/D = 6$ are illustrated in Fig. 2b. The maximum RSS values of 100–650 Pa were observed at $x/D = 6$ and $y/R = 1$. It was apparent that the RSS increases with the jet exit Reynolds numbers. After calculating RSS, we changed the reference coordinates in order to find the RSS_{maj} [23] as shown in Fig. 2c. The maximum value of RSS_{maj} corresponded to the same location where the RSS peaked, as expected. Based on the turbulent kinetic energy dynamic equilibrium, we calculated the turbulent dissipation rate and then determined the TVSS. With the changes in jet exit velocity, maximum TVSS were approximately an order of magnitude less than the RSS_{maj}. The TVSS was mainly distributed along the two sides of the jets in the shear layer regions (Fig. 2d).

Based on the information and contour maps obtained from surveying the jet flow field, the blood samples were aspirated in the vicinity of the lip location where maximum RSS occurred. Figure 3 illustrates the results from the porcine RBC hemolysis experiments. Most data points were taken from flow field locations with the maximum RSS associated with each Reynolds number, but additional RSS values from some of the same Reynolds numbers were included as additional data points to better illustrate the trend of hemolysis. Judging from the data presented in this figure, we may conclude that the incipient stage of hemolysis takes place with RSS of 340 Pa. Below this threshold level, no free-hemoglobin was detectable by our spectrophotometrical method; however, above this threshold, free-hemoglobin showed a monotonic increase corresponding to an increase in the RSS. Based on the studies by Baldwin et al. [23], we modified these stresses to RSS_{maj} to obtain a threshold value of 517 Pa. Using the turbulent dissipation rate to calculate TVSS as described previously, we obtained a threshold value of 60 Pa.

Discussion

In this study, in order to assume dynamic equilibrium, the Reynolds number (Re) must be large enough, the Large scale (L) and Kolmogorov length scale (η) must have a wide range, and the PIV spatial resolution (Δ) must fall within the inertial sub-range; in other words, $L > \Delta \gg \eta$. According to Tennekes and Lumley [12], the flow integral scale for a round jet is approximated by the distance between the center of the jet and the location where the

local mean velocity is half that of the velocity at the jet center. From our mean velocity profile (Fig. 2a), this occurs at $y/R = 1$ and our integral length scale is $L \approx 2$ mm. There is a well-known relation between L/η and the Reynolds number which is $Re \sim (L/\eta)^{4/3}$. In this study, the Large scale (L) was approximately 1.6 mm and the Kolmogorov length scale (η) was roughly 3 μm, making $L/\eta \approx 667$ and therefore $Re \sim 5800$. With our actual Reynolds numbers being much larger ($Re = 25520$–47000), the conditions for assuming dynamic equilibrium are fulfilled and thus making it reasonable to estimate the dissipation rate with the large eddy PIV approach.

In the Smagorinsky model, the Smagorinsky coefficient C_S is a function of L/Δ and Δ/η and is asymptotic to the well-known value of 0.17 when $L/\Delta > 10$ and $\Delta/\eta \geq 100$ [20]. In this study, $L/\Delta \approx 10.5$ and $\Delta/\eta \approx 0.19$ mm/3 μm ≈ 63, approaching 100, thus allowing its use under our experimental conditions. Because PIV does not allow 3-D measurements of the flow fields, the velocity components along the z-axis could not be obtained. When calculating the velocity gradient tensor, 2-D measurement values are substituted under the assumption of isotropicity. However, given that the actual flow fields are anisotropic, we cannot accurately evaluate any direct influences on the results.

Our results revealed that the hemolytic threshold of the RSS_{maj} was up to 517 Pa but the TVSS was <60 Pa. Because the TVSS was not directly measured, we can only compare the results with other studies using different methods. Quinlan and Dooley [16] applied the macroscopic flow parameters by Liu et al. [17] to calculate blood-included loading on individual blood cells. Their results showed that the VSS was smaller than 6 Pa for every model, which is one order smaller than Liu et al.'s RSS of 52 Pa. Antiga and Steinman [18] obtained a VSS of 16 Pa via spectrum elongation, which is on the same order of RSS of 52 Pa by Liu et al. [17]. They used the rms turbulent velocities in the macroscopic scale to estimate the velocity fluctuations in the Kolmogorov eddy scale size, and then determined the spacing of cell–cell interaction under high concentrations of hematocrit. However, since the spectrum data by Liu et al. [17] were not obtained under conditions of high blood cell concentration, and limitations in LDA resolution inherently render the high-frequency side of the spectrum less accurate, the values obtained by Antiga and Steinman [18] still require further investigation and validation.

We applied Eq. (14) to calculate the $TVSS_{2D}$. Our PIV data showed that the threshold $TVSS_{2D}$ was 24 Pa. Calculations from other literature demonstrate that the $TVSS_{2D}$ for hemolysis, from 44 to 380 Pa, tends to be much lower than the RSS threshold, from 250 to 5000 Pa [14]. Because Jones' method was already simplified to two-dimensional flow fields, it is not surprising that there is a difference in magnitude from our values modified to three-dimensional flow fields.

In laminar shear stress experiments, the exposure times are longer at 10^2 s and the hemolysis thresholds ranged between 100 and 300 Pa [1–4], which are several times greater than our TVSS of 60 Pa. Our exposure time was 1.2×10^{-5} s. Even with shorter exposure times of 10^{-4} to 10^{-3} s, other laminar experiments obtained threshold values of 450–560 Pa [5, 6], which are still an order of magnitude larger than our TVSS. It is apparent that the hemolysis threshold differs between laminar and turbulent viscous shear stresses.

Conclusions

Many researchers studying hemolysis across cardiovascular devices considered RSS in turbulence as an important factor. Recently, many studies revealed that TVSS might play an important role in RBC damage. Limited by temporal and spatial resolutions of currently available instrumentation, there has been no detailed study for TVSS in turbulence. In this study, we applied the large eddy PIV method to quantify the TVSS in an attempt to perform a more comprehensive evaluation of the real mechanical force environment relevant to RBC damage in the flow field downstream of the jet. The threshold level of TVSS responsible for incipient hemolysis was found to be approximately 60 Pa. It is one order of magnitude smaller than the RSS_{maj} of 517 Pa. The order of magnitudes certainly matched the results of previous researchers, and it could be considered that using this method provides a proper approximation of the flow field characteristics. The results provide further insight into the relationship between turbulence and red blood cell damage.

Acknowledgments This work was supported by the National Science Council of the Republic of China Grant NSC 100-2221-E-032-012 and we thank the Division of Medical Engineering, National Health Research Institutes of the Republic of China for providing their technical assistance and primary laboratory equipment.

Conflict of interest The authors of this article have no conflicts of interest to disclose.

References

1. Hellums JD, Brown CH. Blood cell damage by mechanical forces. In: Hwang NHC, Normann NA, editors. Cardiovascular flow dynamics and measurements. Baltimore: University Park Press; 1977. p. 799–823.

2. Nevaril CG, Lynch EC, Alfrey CP, Hellums JD. Erythrocyte damage and destruction induced by shearing stress. J Lab Clin Med. 1968;71:784–90.
3. Leverett LB, Hellums JD, Alfrey CP, Lynch EC. Red blood cell damage by shearstress. Biophys J. 1972;12:257–73.
4. Sutera SP, Croce PA, Mehrjardi MH. Hemolysis and subhemolytic alterations of human RBC induced by turbulent shear flow. Trans Am Soc Artif Int Organs. 1972;18:335–41.
5. Williams AR, Hughes DE, Nyborg WL. Hemolysis near a transversely oscillating wire. Science. 1970;169:871–3.
6. Rooney JA. Hemolysis near an ultrasonically pulsating gas bubble. Science. 1970;169:869–71.
7. Forstrom RJ. A new measure of erythrocyte membrane strength: the jet fragility test. PhD. thesis, University of Minnesota; 1969.
8. Sutera SP, Mehrjardi MH. Deformation and fragmentation of human red blood cells in turbulent shear flow. Biophys J. 1975;15:1–10.
9. Sallam AH, Hwang NHC. Human red blood cell hemolysis in turbulent shear flow: contributions of Reynolds shear stresses. Biorheology. 1984;21:783–97.
10. Grigioni M, Daniele C, D'Avenio G, Barbaro V. A discussion on the threshold limit for hemolysis related to Reynolds shear stress. J Biomech. 1999;32:1107–12.
11. Lu PC, Lai HC, Liu JS. A reevaluation and discussion on the threshold limit for hemolysis in a turbulent shear flow. J Biomech. 2001;34:1361–4.
12. Tennekes H, Lumley JL. A first course in turbulence. Cambridge: The MIT Press; 1972.
13. Hinze JD. Turbulence. 2nd ed. New York: McGraw-Hill Book Co.; 1975.
14. Jones SA. A relationship between Reynolds stresses and viscous dissipation: implications to red cell damage. Ann Biomed Eng. 1995;23:21–8.
15. Li CP, Lo CW, Lu PC. Estimation of viscous dissipative stresses induced by a mechanical heart valve using PIV data. Ann Biomed Eng. 2010;38:903–16.
16. Quinlan NJ, Dooley PN. Models of flow-induced loading on blood cells in laminar and turbulent flow, with application to cardiovascular device flow. Ann Biomed Eng. 2007;35:1347–56.
17. Liu JS, Lu PC, Chu SH. Turbulence characteristics downstream of bileaflet aortic valva prostheses. J Biomech Eng. 2000;122:118–24.
18. Antiga L, Steinman DA. Rethinking turbulence in blood. Biorheology. 2009;46:77–81.
19. Sheng J, Meng H, Fox RO. A large eddy PIV method for turbulence dissipation rate estimation. Chem Eng Sci. 2000;55:4423–34.
20. Meyers J, Sagaut P. On the model coefficients for the standard and the variational multi-scale Smagorinsky model. J Fluid Mech. 2006;569:287–319.
21. Hart DP. PIV error correction. Exp Fluids. 2000;29:13–22.
22. Lavoie P, Avallone G, Gregorio FD, Romano GP, Antonia RA. Spatial resolution of PIV for the measurement of turbulence. Exp Fluids. 2007;43:39–51.
23. Baldwin JT, Deutsch S, Petrie HL, Tarbell JM. Determination of principal Reynolds stresses in pulsatile flows after elliptical filtering of discrete velocity measurements. J Biomech Eng. 1993;115:396–403.
24. Liu S, Menenveau C, Katz J. On the properties of similarity subgrid-scale models as deduced from measurements in a turbulence jet. J Fluid Mech. 1994;275:83–119.
25. Smagorinsky J. General circulation experiments with the primitive equation I the basic experiment. Mon Weather Rev. 1963;91:99–164.
26. Zhang T, Fang HB, Jarvik R, Griffith BP, Wu ZJ. Study of the shear-induced blood damage in different species. ASAIO J. 2011;57:122.